Proceedings World Geothermal Congress 2015
Melbourne, Australia, 19-25 April 2015

# Linking TOUGH2 and ABAQUS to Model Permeability Enhancement Using a Damage Mechanics Approach

Justin Pogacnik[1], Mike O'Sullivan and John O'Sullivan

Department of Engineering Science, University of Auckland, Level 3, 70 Symonds St, Auckland 1142, New Zealand

[1]j.pogacnik@auckland.ac.nz

**Keywords:** Irreversible and reversible permeability enhancement, Thermo-Hydro-Mechanical (THM) simulation, cold-water injection, damage mechanics, TOUGH2, ABAQUS.

## ABSTRACT

In geothermal energy production, permeability can be enhanced or inhibited over time by various multiphysics controlled processes such as chemical species dissolution and precipitation, changes in stress or pore pressure, and by temperature effects such as thermal cracking. A wide range of methods has been used to numerically simulate permeability enhancement. Models based on damage mechanics, discrete fracture mechanics, critical shear strain criteria, effective stress, and even empirical permeability multipliers have been proposed in the literature. Previous damage models do not account for the reversible nature of permeability enhancement. During injection, permeability may increase, but during shut-in time, permeability may decrease again. This work seeks to develop a reversible permeability enhancement methodology that is applicable to cyclic injection scenarios for geothermal energy production. Our damage model was implemented in coupled Thermo-Hydro-Mechanical (THM) simulations using AUTOUGH2, the University of Auckland's version of TOUGH2, coupled with the solid mechanics code, ABAQUS. This work offers a step forward and a flexible framework for the modeling of injection-induced damage and permeability enhancement.

## 1. INTRODUCTION

Permeability is one of the most crucial hydrologic parameters and often determines the feasibility of projects involving geologic processes. This is especially true in geothermal energy production. Permeability should be regarding as a time-dependent property that can be enhanced or inhibited over time by various processes such as chemical species dissolution and precipitation, changes in stress or pore pressure, and by temperature effects such as thermal cracking. If permeability is too low, then a geothermal well is often stimulated by over pressurization (hydrofracking or hydroshearing) or injection of cold water to induce thermal cracking and thus enhancing permeability.

A number of works have been published that present coupled multiphysics simulations of both hydrofracking and hydroshearing. Some of the hydrofracking studies include models based on damage mechanics such as Zhou, *et al.* (2006) and Lu, *et al.* (2013). These papers present a coupled hydro-mechanical framework to test damage-induced permeability enhancement models for application to shale oil plays. A noticeable shortcoming in these approaches (for geothermal) is a lack of consideration of thermal effects as well as non-tensile fracture scenarios such as hydroshearing. Pogacnik, O'Sullivan, and O'Sullivan (2014) applied a similar damage mechanics approach to permeability enhancement that included thermal effects for geothermal energy. In that work, permeability evolved as a function of damage and all enhancement was permanent. Other recent examples of shear stimulation simulations with geothermal applications can be seen in the works of Kelkar, *et al.* (2012), Rutqvist, *et al.* (2013), and Dempsey, *et al.* (2013). Rutqvist, *et al.* (2013) used a simplified Coulomb criterion to determine the volume that would be enhanced by shear failure near an injection site. The initiation criterion was simplified so that it effectively became a maximum principal stress criterion. Their work targeted pre-stimulation behavior, and so permeability evolution was not taken into account. Kelkar, *et al.* (2012) and Dempsey, *et al.* (2013) used a Mohr-Coulomb initiation criterion to determine where shear slip should occur near an injection site. Permeability was then altered by either a multiplier (Kelkar, *et al.* (2012)) or by a sigmoidal function (Dempsey, *et al.* (2013)), both designed to approximate the measured permeability data obtained by Lee and Cho (2002). There are also a number of models that use an approach for simulating permeability enhancement by specifying permeability as a function of effective stress (Nathenson (1999) and Pogacnik, *et al.* (2012)). Both the effective stress relationships of Nathenson (1999) and the sigmoidal relationship of Lee and Cho (2002) can trace their roots back to the cubic law of planar fracture flow popularized by Gangi (1978).

Permeability enhancement models in the geothermal sector have lacked the ability to handle both the reversible and the irreversible aspects of permeability enhancement. It is well known that during stimulation, the permeability/injectivity of geothermal wells increases and that after stimulation some of the enhanced permeability is lost, but some permanent enhancement is also retained. Villacorte (2012) studied permeability and injectivity enhancement effects on several geothermal wells in the Philippines and found that some wells showed a reduction in permeability during shut-in time, but that the permeability was still higher than the pre-injection level. Figure 1 was taken from Lee and Cho (2002) and clearly displays both the reversible and irreversible aspects of permeability enhancement during a cyclic shear loading scenario.

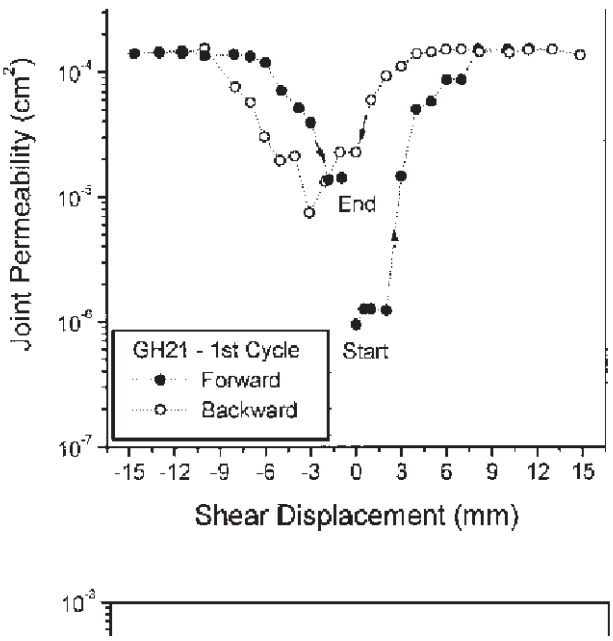


**Figure 1: Permeability enhancement of a rock sample during a cyclic loading scenario (from Lee and Cho (2002)). The figure clearly shows the reversible and irreversible aspects of permeability enhancement. As the specimen is loaded, the permeability increases. However, unloading results in a reduction of a portion of the permeability enhancement, while some permeability enhancement is maintained.**

In this paper, we will present a damage mechanics framework that can be used to capture both the reversible and irreversible aspects of permeability enhancement under cyclic loading. We do this by utilizing AUTOUGH2 to solve the fluid flow and heat transport equations and link those results to ABAQUS for the solid mechanics calculations by using the scripting language, Python. This is an important step in our simulation capability because it provides a link between two robust and advanced numerical solvers that offer the potential to simulate more complex 3D reservoir behavior than has previously been possible.

## 2. BALANCE EQUATIONS

### 2.1 Linear Momentum Balance for the Rock Matrix

Intertial forces in the solid rock matrix were ignored. The linear momentum balance from Bonet and Wood (2008) is written as:

$$\mathrm{div}\boldsymbol{\sigma} + \mathbf{f} = \mathbf{0} \tag{1}$$

where the vector div$\boldsymbol{\sigma}$ is the spatial divergence of the Cauchy stress tensor (to be formally defined in the next section) and **f** a vector of body forces (both external and density related). Note that boldface fonts are used to express matrix and vector quantities. The Cauchy stress can be split into two components to represent the effect of pore fluid pressure on the solid matrix (Lewis and Schrefler (1998); Ingebritsen, Sanford, and Neuzil (2006)):

$$\boldsymbol{\sigma} = \boldsymbol{\sigma}'' - \alpha p \mathbf{I} \tag{2}$$

where $\boldsymbol{\sigma}''$ is Biot's effective stress tensor, $\alpha$ is a constant between 0 and 1, $p$ is the pore fluid pressure, and **I** is the identity tensor. The effective stress is defined by

$$\boldsymbol{\sigma}'' = \mathbf{C}^{\mathrm{D}} : \left(\boldsymbol{\varepsilon} - \boldsymbol{\varepsilon}_T\right) \tag{3}$$

where $\mathbf{C}^{\mathrm{D}}$ is the fourth order material constitutive tensor (to be defined in the next section), $\boldsymbol{\varepsilon}$ is the strain tensor, "**:**" represents the double contraction of two tensors, and $\boldsymbol{\varepsilon}_{\mathrm{T}}$ is the thermal strain tensor given by

$$\boldsymbol{\varepsilon}_T = \left(\beta_S / 3\right)\left(\Delta T\right)\mathbf{I} \tag{4}$$

where $\beta_{\mathrm{S}}$ is the volumetric coefficient of thermal expansion of the solid and $\Delta T$ is the change in temperature from the reference state.

### 2.2 Mass and Energy Balance

The integral form of the mass and energy balance equations for non-isothermal flow in a porous medium can be written as (O'Sullivan *et al.*, 2013):

$$\frac{d}{dt}\int_V A_\kappa dV = -\int_A \mathbf{n}.\mathbf{F}_\kappa dA + \int_V q_\kappa dV \tag{5}$$

where $V$ is the volume of integration, $A_\kappa$ is the amount of each quantity $\kappa$ within the volume, $A$ is the surface of the volume, $\mathbf{F}_\kappa$ is the flux of quantity $\kappa$ across the surface $A$, $\mathbf{n}$ is the normal vector to the surface $A$ and $q_\kappa$ represents any sources or sinks in the control volume. For this study we assume the medium is fully saturated with single-phase water, thus (5) represents conservation equations for mass of water and energy.

The amount of liquid water per unit volume is calculated as shown in Equation (6):

$$A_l = \varphi(\rho_l) \tag{6}$$

Here $\varphi$ is the porosity and $\rho_l$ is the density. The liquid phase is indicated by the subscript $l$. For the amount of energy per unit volume the formula includes an additional term for the contribution of the rock:

$$A_e = (1-\varphi)\rho_r c_r T + \varphi(\rho_l u_l) \tag{7}$$

Here $T$ is the temperature, $\rho_r$ the density of the rock, $c_r$ its heat capacity and $u_l$ the internal energy of the liquid. The flux of energy $\mathbf{F}_e$ in Equation (5) is calculated by:

$$\mathbf{F}_e = h_l \mathbf{F}_l - K\nabla T \tag{8}$$

where $K$ is the thermal conductivity, $h_l$ is the enthalpy of the liquid, and $\mathbf{F}_l$ is the liquid flux. In most geothermal systems the effects of diffusion and hydrodynamic dispersion are small and the flux of the liquid is given by Darcy's Law:

$$\mathbf{F}_l = -\frac{\boldsymbol{\kappa}}{\nu_l}\left(\nabla p + \rho_l \mathbf{g}\right) \tag{9}$$

Here $\boldsymbol{\kappa}$ is the permeability tensor, $\nu_l$ is kinematic viscosity, $p$ the pressure and $\mathbf{g}$ is gravity.

## 3. CONSTITUTIVE EQUATIONS

### 3.1 Isotropic Elasticity-based Damage

We implement a simple isotropic elasticity-based damage model that is based on Section 6.2 in De Borst, *et al.* (2012). This type of damage model is simple to implement and allows us to capture more advanced material behavior such as stress-strain softening and failure. In this approach, the damage variable is represented by the scalar variable, $D$ that ranges from 0 in the case of no damage to 1 in the case of a fully damaged volume.

In 3D, the fourth order elasticity tensor of Equation (3) can be recast in matrix form as:

$$C^D = (1-D)\frac{E}{(1+\upsilon)(1-2\upsilon)}\begin{bmatrix} 1-\upsilon & \upsilon & \upsilon & 0 & 0 & 0 \\ \upsilon & 1-\upsilon & \upsilon & 0 & 0 & 0 \\ \upsilon & \upsilon & 1-\upsilon & 0 & 0 & 0 \\ 0 & 0 & 0 & \frac{1-2\upsilon}{2} & 0 & 0 \\ 0 & 0 & 0 & 0 & \frac{1-2\upsilon}{2} & 0 \\ 0 & 0 & 0 & 0 & 0 & \frac{1-2\upsilon}{2} \end{bmatrix} \tag{10}$$

where $E$ is Young's modulus and $\upsilon$ is Poisson's ratio. So, it can be seen that in the case of maximum damage, $D$=1, the material exhibits no resistance to deformation and is completely failed.

In this work, damage evolves as a function of a strain energy measure presented in De Borst, *et al.* (2012) and, Pogacnik, O'Sullivan, and O'Sullivan (2014). The strain energy measure is defined as

$$\tilde{\varepsilon} = \sqrt{\frac{1}{E}\boldsymbol{\varepsilon} : \mathbf{C}^e : \boldsymbol{\varepsilon}} \tag{11}$$

where $\mathbf{C}^e$ is the elastic stiffness tensor, given by Equation (10) with $D$=0. $D$ can be cast as a piecewise continuous function of the strain energy measure:

$$D = \begin{cases} 0 & \text{if} \quad \tilde{\varepsilon} < \tilde{\varepsilon}_c \\ \dfrac{D_{\text{off}}}{\tilde{\varepsilon}_{\text{off}} - \tilde{\varepsilon}_c}\tilde{\varepsilon} - D_{\text{off}}\dfrac{\tilde{\varepsilon}_c}{\tilde{\varepsilon}_{\text{off}} - \tilde{\varepsilon}_c} & \text{if} \quad \tilde{\varepsilon}_c \le \tilde{\varepsilon} \le \tilde{\varepsilon}_{\text{off}} \\ D_{\text{lim}} - \left(D_{\text{lim}} - D_{\text{off}}\right)\dfrac{\tilde{\varepsilon}_{\text{off}}}{\tilde{\varepsilon}} & \text{if} \quad \tilde{\varepsilon} > \tilde{\varepsilon}_{\text{off}} \end{cases} \tag{12}$$

where $\tilde{\varepsilon}_c$ represents the critical value of the strain energy where damage begins; $\tilde{\varepsilon}_{\text{off}}$ is a cutoff value of the strain energy measure that corresponds to damage equal to $D_{\text{off}}$; and $D_{\text{lim}}$ is the limiting value of damage (theoretically $D_{\text{lim}}$=1, though lower values could be used to match experimental data).

**3.2 Permeability Evolution**

In this work, we formulate permeability to be a function of both strain and damage in a cumulative relationship:

$$\boldsymbol{\kappa} = \kappa_\varepsilon \mathbf{I} + \kappa_D \mathbf{I} \tag{13}$$

where $\kappa_\varepsilon$ is the strain-controlled portion of permeability and $\kappa_D$ is the damage-controlled portion of permeability. The strain-controlled portion of the permeability tensor is the reversible part. An increase in the strain energy measure will result in an increase in permeability and a decrease in the strain energy measure results in a decrease in permeability. Damage is permanent, therefore, that portion of the permeability tensor represents irreversible permeability enhancement. We define both the strain- and damage-dependent portions of the permeability tensor by sigmoidal relationships as in Lee and Cho (2002), Dempsey, *et al.* (2013) and Pogacnik, O'Sullivan, and O'Sullivan (2014):

$$\kappa_\varepsilon = \frac{\kappa_0}{2} + \left[\frac{\kappa_{\max}/2 - \kappa_0/2}{1 + \exp\left[-\lambda_\varepsilon\left(\tilde{\varepsilon} - \tilde{\varepsilon}_{\text{on}}\right)\right]}\right] \tag{14}$$

and

$$\kappa_D = \frac{\kappa_0}{2} + \left(\frac{\kappa_{\max}/2 - \kappa_0/2}{1 + \exp\left[-\lambda_D\left(D - D_{\text{on}}\right)\right]}\right) \tag{15}$$

where $\lambda_{\varepsilon,D}$, $D_{\text{on}}$, and $\tilde{\varepsilon}_{\text{on}}$ are curve-fit parameters to match experimental and/or field data; $\kappa_0$ is the original permeability prior to stimulation; and $\kappa_{\max}$ is the maximum permeability. We apply equal weight to both the damage-permeability and strain-permeability portions. It is the subject of future study to determine how to apply these relationships to best match field and experimental data. Figure 2 displays the theoretical behavior predicted by Equations (11) - (15) for a uniaxial cyclic strain scenario similar to the results presented by Lee and Cho (2002) in Figure 1. In this case, the strain is first tensile (black dots), then compressive to the same strain level (white dots). This shows that on the return to zero strain, there has been some permanent permeability enhancement.

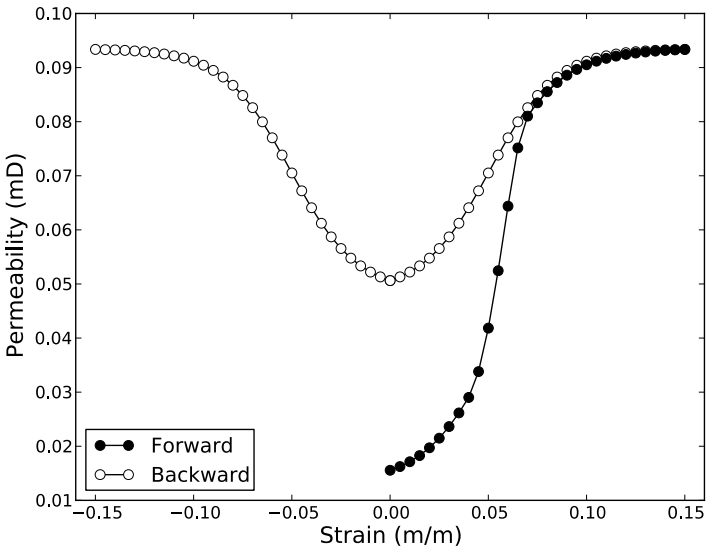


**Figure 2. This figure displays the theoretical strain-permeability curve for this model when Equations (11)-(15) are applied to a cyclic loading scenario. In forward loading, the permeability increases, however subsequent unloading does not result in a complete recovery of the enhanced permeability. Further reverse loading enhances permeability back to the same level as the forward loading portion. This behavior is qualitatively similar to that provided by Lee and Cho (2002) in Figure 1.**

## 4. NUMERICAL PROCEDURE

In this work, we coupled TOUGH2 for heat and fluid transport to ABAQUS for solid mechanics. Coupling these two extensive codes allows for the potential of larger problem sizes and more advanced physical phenomena to be modeled than is possible with current THM codes. The TOUGH2/ABAQUS combination was previously used at the University of Auckland for modelling subsidence (O'Sullivan and Yeh, 2007; Bromley *et al.*, 2010). However subsidence is a much slower process than those considered here and a much looser coupling between the heat and mass transfer and the rock mechanics was possible.

Various THM studies have used TOUGH2 coupled with the commercial rock mechanics code FLAC3D (Rutqvist *et al.* 2002, 2006). The originators of the TOUGH2/FLAC3D combination coined the name TOUGH-FLAC (Rutqvist, 2011) for the coupled codes. TOUGH-FLAC has not been used for investigating the damage models discussed here.

We coupled TOUGH2 and ABAQUS through the use of the scripting language Python. This was a natural choice due to the extensive development of the PyTOUGH (Croucher, (2011)) library at the University of Auckland for interfacing with the TOUGH2 simulator and since Python is the standard programming language of ABAQUS and offers the most efficient way to access ABAQUS' output (Output Database – *.odb). Figure 3 displays a pseudo Python code used in this work to run these coupled simulations.

```
· Import necessary Python libraries
· Define filenames/paths for each code's executable/input/output/etc.
· Define material properties
for t in timesteps do
    · Use PyTOUGH to setup and run TOUGH2 simulation for pressures
      and temperatures
    · Setup and write Abaqus input file
    · Execute Abaqus simulation for displacements/stresses
    · Postprocess results
    · Compute damage from ε̃
    · Update permeability (κ) and Young's Modulus (E)
end
```

**Figure 3. Pseudo Python code used to couple TOUGH2 to ABAQUS for the simulations in this work.**

This approach would be classified as a Sequential Non-Iterative Approach (SNIA). This means that after the computation of the damage and new material parameters, the simulation marches on in time. From Pogacnik, Dempsey, *et al.* (2014), this type of approach can result in incorrect pressure calculations at small times due to the strong feedback of the solid mechanics equations to the flow equations through permeability enhancement.

We set up the ABAQUS simulation by first accessing the TOUGH2 simulation results using PyTOUGH. Care has to be taken to convert the TOUGH2 geometry into a finite element mesh. Our current capability is limited to 3D rectangular domains where the

TOUGH2 grid and the finite element mesh exactly correspond. The pressures and temperatures from the TOUGH2 simulation were enforced in ABAQUS as Dirichlet boundary conditions over every node in the domain with the "*BOUNDARY, FIXED" command in the input file. In order to accommodate spatially varying material properties, we defined a separate rock-type for each block in TOUGH2 and a separate element set (*ELSET) and material type (*MATERIAL) for each finite element in ABAQUS. The element types used in ABAQUS were "C3D8PT" which are **C**ontinuum **3D** elements with **8** nodes that include pore **P**ressure and **T**emperature. The next section will detail the boundary value problem for the numerical simulation used in this work.

## 5. SIMULATION SETUP

For numerical simulation, we tested a simple pseudo 1D column. This was an appropriate choice to verify the permeability enhancement relationship while also allowing for our first step in coupling two advanced numerical codes. The column boundary value problem was set up to approximate a cold-water injection scenario at about 1km depth in a geothermal field. Figure 4 displays the meshed domain used in this work.

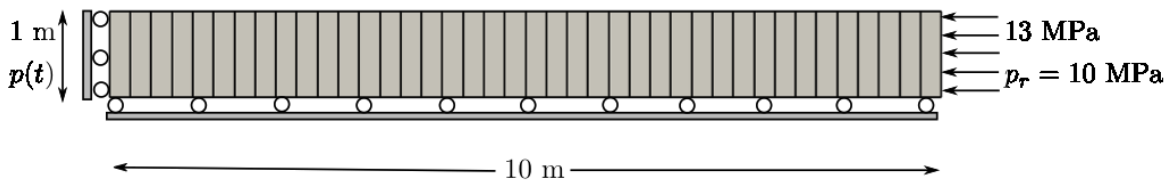


**Figure 4. The figure displays the pseudo 1D column used in this work. The grid was actually a 1m x 1m x 10 m 3D column with only a single element block in the first two coordinate directions. The domain was initially at 200°C and with 10 MPa pore fluid pressure. Cold water of 100°C was injected at the left hand side at a recharge pressure given in Figure 5.**

The geometry was 1m x 1m x 10m and the initial temperature and pressure were 200°C and 10.0 MPa, respectively. The material parameters used in this study are presented in Table 1.

| Parameter | Symbol | Value | Units |
|---|---|---|---|
| Rock Density | $\rho_s$ | 2000.0 | $\mathrm{kg/m^3}$ |
| Young's Modulus | $E$ | $20 \times 10^9$ | Pa |
| Poisson's Ratio | $\nu$ | 0.25 | - |
| Porosity | $n$ | 0.10 | - |
| Rock Coefficient of Thermal Expansion | $\beta_s$ | $5.5 \times 10^{-5}$ | 1/°C |
| Rock Specific Heat | $c_s$ | 1000.0 | J/kg °C |
| Rock Thermal Conductivity | $\chi_s$ | 1.5 | W/m°C |
| Biot Coefficient | $\alpha$ | 1.0 | - |
| Initial Permeability | $\kappa_0$ | $1.0 \times 10^{-14}$ | $\mathrm{m^2}$ |
| Max Permeability | $\kappa_{\max}$ | $1.0 \times 10^{-13}$ | $\mathrm{m^2}$ |
| - | $\lambda_\varepsilon$ | 10000 | - |
| - | $\tilde{\varepsilon}_{\mathrm{on}}$ | 0.03 | - |
| - | $\lambda_D$ | 15.0 | - |
| - | $D_{\mathrm{on}}$ | 0.4 | - |
| - | $\tilde{\varepsilon}_c$ | 0.028 | - |
| - | $\tilde{\varepsilon}_{\mathrm{off}}$ | 0.035 | - |
| - | $D_{\mathrm{off}}$ | 0.8 | - |
| - | $D_{\mathrm{lim}}$ | 0.9 | - |

**Table 1. Values of material parameters used in this study.**

Cold water was injected at the left hand side by using a recharge well type in TOUGH2. The recharge pressure varied over time and can be seen in Figure 5. The injection pressure profile includes shut-in times where no well overpressure occurs.

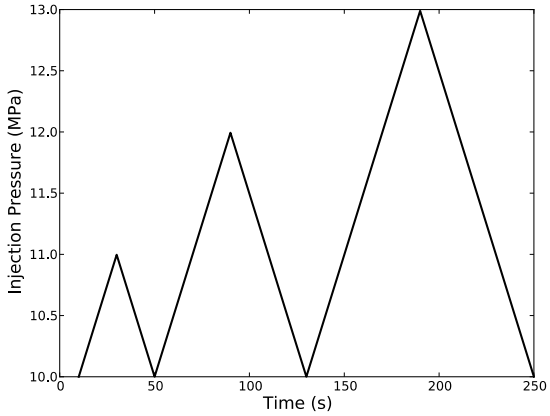


**Figure 5. The injection pressure at the left hand side of the 1D column as a function of time includes time where there is no well overpressure.**

## 6. RESULTS AND DISCUSSION

Figure 6 displays the result for damage as a function of time for an arbitrary element located 1m from the left hand side of the domain. Figure 7 displays the permeability result for the same element. In these figures, the horizontal stress was fixed, while injection pressure was varied over time as shown in Figure 5. The increased injection pressure resulted in permanent damage in the element that in turn led to permanent permeability enhancement. However, upon pressure reduction, the strain-controlled portion of the enhanced permeability was lost, however the damage done was permanent and did not reduce. This behavior is clearly seen in Figures 6 and 7. Subsequent pressurizations led to higher damage levels and thus, higher permeability levels. Notice that each cycle shows a slight increase in the permeability when compared to the previous cycle. We do not have access to any data to compare with these simulation results. The purpose of this simulation was to show that this framework is capable of simulating both reversible and irreversible aspects of permeability enhancement. These results are very sensitive to the parameters chosen to populate Equations (12)-(15). It will be necessary to calibrate this empirical model on a wide range of experimental and field data to use it for large-scale reservoir simulations.

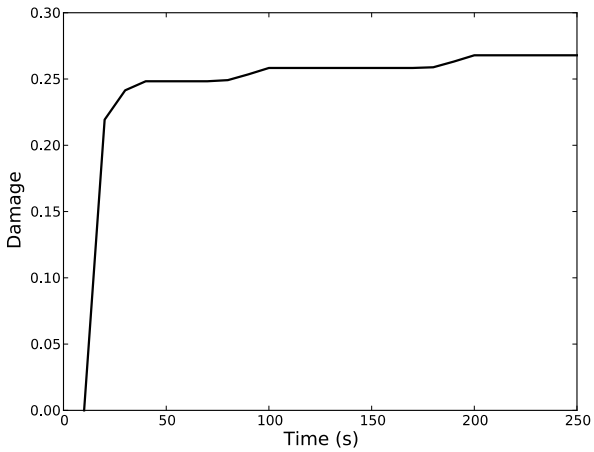


**Figure 6. The figure displays damage as a function of time for the 1D column injection scenario. Since damage is irreversible, it does not decrease upon subsequent pressure reduction periods.**

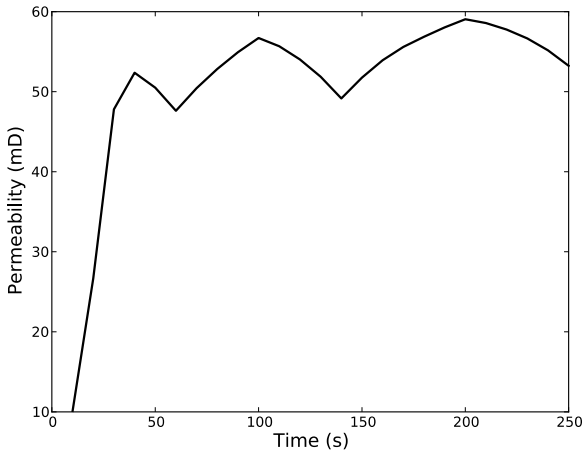


**Figure 7. The figure displays permeability as a function of time for the 1D column injection scenario. Permeability increases as a result of injection pressure and damage. When pressure is reduced, the permeability decreases some, but not fully due to permanent strain-induced damage that has occurred in the rock.**

## 7. SUMMARY AND FUTURE WORK

In this work, we first present a damage mechanics approach to modeling permeability enhancement that has both reversible and irreversible effects. Upon injection and an increase in stored strain energy, damage occurs in the rock that enhances permeability. When injection stops and fluid pressure returns to the natural state level, permeability decreases, however the damage is permanent, and so a portion of the enhanced permeability is also permanent. It is not clear if this relationship is the appropriate relationship, however, it is an empirical model that is capable of matching the physical behavior we see in the limited data that we have access to (see Figures (1) and (2)). We hope to further calibrate and test this framework with experimental data in the near future.

We have also coupled AUTOUGH2 with ABAQUS for application to THM simulations for geothermal energy. While the boundary value problem presented here was simple, coupling these two robust numerical solvers offers the potential to solve complex reservoir heat and fluid flow problems with advanced solid mechanics constitutive behavior in large 3D simulations. We have a framework in place that allows for a Sequential Non-Iterative solution approach to couple the two codes. We are working to extend our simulation capability significantly on this front. Specifically, we seek to: include an iterative solution procedure that will better solve the equilibrated balance equations at each time step; utilize ABAQUS extensive solid mechanics constitutive library and capabilities for complex rock behaviors; and to allow the user to perform solid mechanics solutions on a portion of the TOUGH2 grid, instead of the entire domain.

## ACKNOWLEDGEMENTS

The authors wish to gratefully acknowledge GNS in New Zealand for their support of this work at the University of Auckland.

## REFERENCES

Bromley, C.J, Currie, S., Ramsay, G., Rosenberg, M., Pender, M., O'Sullivan, M., Lynne, B., Lee, S-G., Brockbank, K., Glynn-Morris, T., Mannington, W., & Garvey, J.: Tauhara Stage II Geothermal Project: Subsidence Report, GNS Science Consultancy Report 2010/151 (and appendices 1-10). Published by Contact Energy Ltd. 154p, (2010).

Croucher, A: PyTOUGH: A Python Scripting Library for Automating TOUGH2 Simulations, *Proceedings*, New Zealand Geothermal Workshop, (2011).

DeBorst, R., Crisfield, A., *et al.*: *Nonlinear Finite Element Analysis of Solids and Structures*, John Wiley and Sons Ltd, (2012).

Dempsey, D., Kelkar, S., Lewis, K, *et al.*: Modeling Shear Stimulation of the Desert Peak EGS Well 27-15 Using a Coupled Thermal-Hydrological-Mechanical Simulator, *47th US Rock Mechanics/Geomechanics Symposium*, San Francisco, CA, USA (2013).

Gangi, A.: Variation of Whole and Fractured Porous Rock Permeability with Confining Pressure, *International Journal of Rock Mechanics, Mineral Science, and Geomechanics*, **15**, (1978), 249-257.

Kelkar, S., Lewis, K., Hickman, S., *et al.*: Modeling Coupled Thermal-Hydrological-Mechanical Processes During Shear Stimulation of an EGS Well, *Proceedings*, 37th Workshop of Geothermal Reservoir Engineering, Stanford University, Stanford, CA, (2012).

Lee, H. and Cho, T.: Hydraulic Characteristics of Rough Fractures in Linear Flow under Normal and Shear Load, *Rock Mechanics and Rock Engineering*, **35 (4)**, (2002), 299-318.

Lu, Y., Elsworth, D., and Wang, L.: Microcrack-based Coupled Damage and Flow Modeling of Fracturing Evolution in Permeable Brittle Rocks, *Computers and Geotechnics*, **49**, (2013), 226-244.

Nathenson, M.: The Dependence of Permeability on Effective Stress from Flow Tests at Hot Dry Rock Reservoirs at Rosemanowes (Cornwall) and Fenton Hill (New Mexico), *Geothermics*, **28**, (1999), 315-340.

O'Sullivan J., Croucher, A., Yeh, A. and O'Sullivan M.J.: Improved convergence for air-water and CO2-water TOUGH2 simulations. *Proceedings,* New Zealand Geothermal Workshop, Rotorua, New Zealand, (2013).

Pogacnik, J., Leary, P., and Malin, P.: Physical/Computational Framework for EGS *in situ* Fracture Stimulation, *Proceedings*, New Zealand Geothermal Workshop, (2012).

Pogacnik, J., O'Sullivan, M., and O'Sullivan, J.: A Damage Mechanics Approach to Modeling Permeability Enhancement in Thermo-Hydro-Mechanical Simulations, *Proceedings*, Thirty-Ninth Workshop on Geothermal Reservoir Engineering, Stanford University, Stanford, CA, USA, February 24-26, (2014).

Pogacnik, J., Dempsey, D., Kelkar, S, *et al.*: The Effect of Sequential Solution Procedures in the Numerical Modeling of Stimulation in Engineered Geothermal Systems, *Proceedings*, 11th World Congress on Computational Mechanics, Barcelona, Spain, (2014).

Rutqvist, J.: Status of the TOUGH-FLAC simulator and recent applications related to coupled fluid flow and crustal deformations. *Computers & Geosciences* **37,** (2011), 739–750.

Rutqvist, J., Wu, Y.-S, Tsang, C.-F. and Bodvarsson, G.: A modelling approach for analysis of coupled multiphase fluid flow, heat transfer, and deformation in fractured porous rock, *International Journal of Rock Mechanics*, **39**, (2002), 429–442.

Rutqvist, J., Birkholzer, J., Cappa, F.d.r., Oldenburg, C. and Tsang, C.-F.: Shear-slip analysis in multiphase fluid-flow reservoir engineering applications using TOUGH-FLAC. *Proceedings*, TOUGH Symposium Lawrence Berkeley National Laboratory, Berkeley, California, (2006).

Rutqvist, J., Dobson, P., Garcia, J., *et al.*: Pre-Stimulation Coupled THM Modeling Related to the Northwest Geysers EGS Demonstration Project, *Proceedings*, 38th Workshop of Geothermal Reservoir Engineering, Stanford University, Stanford, CA (2013).

Villacorte, J.: *Injection Tests Analysis Using Inverse Modelling*. M.Sc. Thesis, University of Auckland, New Zealand (2012).

Yeh, A. and O'Sullivan, M.J.: Computer modelling subsidence in geothermal fields, *Proceedings,* 29th New Zealand Geothermal Workshop, University of Auckland. (2007).

Zhou, J. Shao, J., Xu, W.: Coupled Modeling of Damage Growth and Permeability Variation in Brittle Rocks, *Mechanics Research Communications*, **33**, (2006), 450-459.